HHS Public Access

Author manuscript

Bioelectrochemistry. Author manuscript; available in PMC 2023 March 25.

Published in final edited form as:

Bioelectrochemistry. 2020 February ; 131: 107369. doi:10.1016/j.bioelechem.2019.107369.

Understanding the role of calcium-mediated cell death in high-frequency irreversible electroporation

Elisa M. Wasson[a,e,*], **Nastaran Alinezhadbalalami**[b,e], **Rebecca M. Brock**[c,d], **Irving C. Allen**[c,d,e], **Scott S. Verbridge**[b,e], **Rafael V. Davalos**[a,b,e]

[a]Department of Mechanical Engineering, Virginia Tech, Goodwin Hall, 635 Prices Fork Road, Blacksburg, VA, 24061, USA

[b]Department of Biomedical Engineering and Mechanics, Virginia Tech- Wake Forest University, 325 Stanger Street, Blacksburg, VA, 24061, USA

[c]Graduate Program in Translational Biology, Medicine, and Health, Virginia Tech, 1 Riverside Circle, Roanoke, VA, 24016

[d]Department of Biomedical Sciences and Pathobiology, Virginia Tech, 205 Duck Pond Drive, Blacksburg, VA, 24061, USA

[e]Institute for Critical Technology and Applied Sciences Center for Engineered Health, Virginia Tech, Kelly Hall, Blacksburg, VA, 24061, USA

Abstract

High-frequency irreversible electroporation (H-FIRE) is an emerging electroporation-based therapy used to ablate cancerous tissue. Treatment consists of delivering short, bipolar pulses (1–10 μs) in a series of 80–100 bursts (1 burst/second, 100 μs on-time). Reducing pulse duration leads to reduced treatment volumes compared to traditional IRE, therefore larger voltages must be applied to generate ablations comparable in size. We show that adjuvant calcium enhances ablation area in vitro for H-FIRE treatments of several pulse durations (1, 2, 5, 10 μs). Furthermore, H-FIRE treatment using 10 μs pulses delivered with 1 mM $CaCl_2$ results in cell death thresholds (771 ± 129 V/cm) comparable to IRE thresholds without calcium (698 ± 103 V/cm). Quantifying the reversible electroporation threshold revealed that $CaCl_2$ enhances the permeabilization of cells compared to a NaCl control. Gene expression analysis determined that $CaCl_2$ upregulates expression of eIFB5 and 60S ribosomal subunit genes while downregulating NOX1/4, leading to increased signaling in pathways that may cause necroptosis. The opposite was found for control treatment without $CaCl_2$ suggesting cells experience an increase in pro survival signaling. Our study is the first to identify key genes and signaling pathways responsible for differences in cell response to H-FIRE treatment with and without calcium.

[*]**Corresponding author.** EMW – ewasson1@vt.edu.

Keywords

irreversible electroporation (IRE); high-frequency irreversible electroporation (H-FIRE); calcium; enhanced ablation; reversible electroporation; cell death

1. Introduction

Irreversible electroporation (IRE) treatment is an alternative to standard cancer therapies which has been shown to successfully treat the most aggressive, and sometimes unresectable tumors such as pancreatic adenocarcinoma in human patients [1–4] as well as glioblastoma in canine patients [5–8]. In a typical electroporation treatment, needle electrodes are inserted into the tumor and a series of electrical pulses are delivered to the tissue. The applied electric field induces a rise in the cells' transmembrane potential (TMP). This rise in TMP lowers the energy needed for hydrophilic pores to form in the membrane [9,10] in a phenomenon known as electroporation. These pores allow otherwise impermeable molecules and ions to enter the cell. Additionally, recent studies have shown that voltage gated channels may affect transport during electroporation, also allowing exchange of molecules [11] that may lead to a loss of cellular homeostasis. Pulse parameters that are applied (field strength, pulse duration, and number of pulses) can be varied to elicit different cellular responses. Below a critical energy threshold, cells can recover from the loss of homeostasis and the pores may reseal over time. The cells are then said to experience reversible electroporation. Taking advantage of the enhanced cell membrane permeability and transport into the cell, reversible electroporation has commonly been used in gene transfer [12,13] as well as for the treatment of tumors in a technique known as electrochemotherapy (ECT) [14–17]. However, if the applied energy surpasses the critical threshold, cells cannot recover from the loss of homeostasis induced by the electrical field. The permanent loss of homeostasis results in cell death and cells are said to experience irreversible electroporation. IRE has been shown to cause minimal thermal damage to tissue [18], unlike techniques such as radiofrequency and microwave ablation, therefore sparing critical structures such as vasculature and nerves [19,20].

Despite the promising outlook of IRE for treatment of unresectable tumors [21], clinical application of IRE is known to cause muscle contractions in human and animal patients, requiring the use of neuroparalytic agents [22,23]. We have developed a second generation modality of IRE treatment known as high-frequency irreversible electroporation (H-FIRE) to address these limitations [24]. While traditional IRE treatment uses square, unipolar pulses of 100 μs, H-FIRE treatment uses bipolar pulses that are much shorter in duration (1–10 μs) and are delivered in a series of 80–100 bursts (1 burst/second), as in the case of IRE (1 pulse/second). It has been hypothesized that delivering pulses at a higher frequency diminishes the dependence of IRE on cell size and tissue geometry [25–27]. Nonlinear changes in tissue conductivity occur to a lesser degree than in IRE treatment [28,29] and therefore ablations using H-FIRE have been shown to be more predictable and uniform [30,31]. H-FIRE treatment also mitigates muscle contractions seen with IRE treatment [24]. However, reducing pulse duration in H-FIRE treatment leads to a reduction in treatment volume compared to traditional IRE. This necessitates the use of much larger applied

voltages to generate ablations comparable in size. Higher voltages may increase thermal damage and the likelihood of inducing muscle contractions [31–33], therefore negating some of the benefits that H-FIRE treatment has over traditional IRE.

It has been shown that utilizing ECT pulses in combination with adjuvant calcium results in ATP depletion of cancer cells for as long as eight hours after treatment, compared to only one hour after electroporation treatment alone, leading to enhanced cell death [34–38]. Motivated by these studies, we have previously demonstrated that using adjuvant calcium in combination with IRE treatment induces a larger zone of cell death without the need to increase the energy applied to the tissue [39]. We hypothesize that using adjuvant calcium will enhance the lethality of H-FIRE treatment. Utilizing adjuvant calcium with H-FIRE treatment will allow us to retain its clinical advantages while eliminating the need to use higher voltages to produce ablations similar in size to traditional IRE treatment.

We investigated our hypothesis using a simplified collagen hydrogel model of a tumor that allowed visualization of treatment ablations. Cancer cells were seeded in collagen scaffolds and treated using H-FIRE waveforms of varying pulse durations (1, 2, 5, and 10 μs) with and without calcium. Reversible and irreversible electroporation thresholds were quantified and compared to our previously tested calcium IRE treatments [39] to elucidate differences in cell death response to extracellular calcium. Finally, we began work to uncover the biological effects on cells in response to H-FIRE treatment with and without calcium, which to our knowledge, has not been previously investigated. Our results show that adjuvant calcium enhances ablation size for all H-FIRE treatments. Furthermore, 10 μs pulses delivered with calcium result in ablations comparable in size to IRE treatment without calcium. Additional mechanistic studies identified signaling pathways associated with NADPH oxidase activity, ROS production, and the translation of stress related mRNA that were differentially dysregulated under $CaCl_2$ and no $CaCl_2$ conditions, impacting cell death.

2. Materials and Methods

2.1 Cell culture

U251 malignant glioma cells (Sigma Aldrich, 09063001) were maintained at 5% CO_2 and 37°C in Eagle's Minimum Essential Medium (Sigma Aldrich) supplemented with 1% penicillin/streptomycin (Life Technologies), 10% fetal bovine serum (Atlanta Biologicals), 1% non-essential amino acids (Sigma Aldrich) and 1 mM sodium pyruvate (Sigma Aldrich). Cells were routinely passaged at 80–90% confluence.

2.2 Collagen scaffold preparation

Sterile polydimethylsiloxane (PDMS, SYLGARD™ 184, Dow Corning) wells (10 mm diameter, 1 mm height) were placed in a 24 well plate to ensure uniform collagen scaffold geometry and electric field distribution between each replicate. PDMS wells were treated with 1% PEI (Acros Organics) for 10 minutes, 0.1% glutaraldehyde (Fisher Scientific) for 20 minutes, and then washed twice with deionized water prior to collagen seeding to ensure collagen adhesion during treatment. Commercial rat tail collagen type I (BD

Biosciences) was neutralized using a solution of 10X Dulbecco's Modified Eagle Medium (10% total volume, Sigma Aldrich), 1 N NaOH (2% collagen volume, Sigma Aldrich), and 1X Dulbecco's Modified Eagle Medium (Sigma Aldrich) to a final concentration of 5 mg/mL. U251 cells were detached from flasks using 0.25% trypsin/EDTA (Thermo Fisher Scientific) solution and added to the neutralized collagen solution at a concentration of 1×10^6 cells/mL. The collagen/cell solution was dispensed into PDMS wells and PDMS tops were used to mold the collagen flat while they polymerized in a cell culture incubator for 20 minutes. PDMS tops were removed and cell culture media was added. Collagen scaffolds were maintained in the incubator for 24 hours prior to treatment.

2.3 Electroporation treatment

After 24 hours, the media was aspirated from scaffolds and replaced with either $CaCl_2$ (Fisher Scientific) or NaCl (Fisher Scientific) solutions (1 mM or 5 mM). Each solution contained the same base components; 250 mM sucrose (Fisher Scientific), 1 mM $MgCl_2$ (Sigma Aldrich) and 10 mM HEPES buffer (Sigma Aldrich) in deionized water with pH of 7.2–7.4. Supplementary Table I lists the osmolarity and conductivity of buffers used in this study. Solutions incubated in the wells at room temperature for 30 minutes, were aspirated, and then replaced with fresh $CaCl_2$ or NaCl solutions for another 10 minutes to ensure that all media was removed. Fresh solutions were added immediately prior to pulsing. A custom-designed electrode housing was used to ensure precise placement (4 mm center-to-center spacing) of two hollow, stainless-steel blunt tip needles with 0.914 mm outer diameter and 0.635 mm inner diameter (Howard Electronic Instruments) into the collagen scaffold. To investigate whether enhanced cell death was unique to calcium, other ions that are involved in removing calcium from the cell were tested, namely KCl (1 mM, Alfa Aesar) and a combination of $CaCl_2$ and NaCl (1 mM each). These treatments followed the same protocol described above.

Several H-FIRE pulses were investigated in this study and delivered using a custom-built pulse generator (EPULSUS®-FBM1–5, EnergyPulse Systems, Lda). Waveforms were captured using a voltage probe (BTX, Harvard Apparatus) and oscilloscope (DPO 2012, Tektronix). An H-FIRE waveform can be described by pulse duration, inter-pulse delay, number of pulses, number of bursts, and frequency of burst delivery (Schematic 1). Here, we describe the treatment delivered by the parameters of one bipolar pulse (positive pulse duration, inter-pulse delay, and negative pulse duration). Inter-pulse delay was kept constant at 1 μs while pulse duration was varied (1, 2, 5, and 10 μs). 80 bursts with a total on-time of 100 μs (100, 50, 20 and 10 pulses consecutively) were delivered at a frequency of 1 burst/sec and a voltage of 800 V. For irreversible threshold experiments, $CaCl_2$ and NaCl solutions were aspirated and replaced with cell culture media and scaffolds were returned to the incubator for 24 hours prior to live/dead staining. For reversible threshold experiments, scaffolds were imaged immediately after treatment as described below.

2.4 Analysis of ablation area

To visualize ablations, scaffolds were stained with calcein AM and propidium iodide (PI). It has been previously determined that 24 hours post treatment is sufficient to allow any reversibly electroporated cells to recover as pore resealing happens on the order of minutes

[40,41], therefore, staining the cells immediately after treatment and 24 hours later allows us to quantify both the reversible zone of electroporation and irreversible zones of ablation. To stain the scaffolds, media was removed and replaced with phosphate buffered saline (PBS) containing 2 μM calcein AM (Invitrogen) and 23 μM PI (Invitrogen) and incubated at room temperature for 30 minutes. Scaffolds were then washed twice with PBS prior to imaging using an inverted microscope (DMI 6000B, Leica Microsystems) with a 5x objective, filter cubes with and an EMCCD camera (Hamamatsu C9100). The appropriate filters were used to image Calcein AM (Ex:460–500; DC: 505; EM: 570–640) and propidium iodide (EX:545/26, DC:565, EM:605/70). To determine the reversible zone of electroporation, treatment followed the same electroporation protocol described above, but calcein AM and PI were added to the $CaCl_2$ and NaCl solutions at all steps prior to pulsing. Scaffolds were then imaged immediately after treatment.

For analysis, images were separated into two channels (green – calcein AM, red – PI) and ablation areas for the green channel were analyzed for irreversible thresholds and red channels for reversible electroporation thresholds using a custom algorithm written in MATLAB as previously described [39]. In cases where the algorithm was unable to accurately measure ablations, coordinate points from the algorithm outlining the ablation area were used as a guide to manually trace and measure the area in ImageJ. Ablation area measurements were mapped to a finite element model of the experimental setup to determine the corresponding electric field threshold. These methods have been previously reported [39,42,43] and are detailed in Supplementary Material.

2.5 Gene Expression Analysis

Collagen scaffolds, prepared as previously described, were subjected to 5 mM $CaCl_2$ (n = 10) or 5 mM NaCl (n = 10) solutions as described above. Wells were treated with either 2–1-2 or 10–1-10 H-FIRE waveforms while submerged with solution buffers. Treated wells were rested for 24 hours in media and then underwent collagenase digestion for cell retrieval. 0.5% collagenase (Thermo Fisher) and 1% fetal bovine serum (Atlanta Biologicals) in Hanks Buffered Salt Solution (HBSS) (Lonza) were added to each well. The samples were then incubated at 37°C for 2 hours. Recovered cells were washed with ice cold PBS. Scaffolds were pooled by group and RNA extracted using TRIzol (ThermoFisher). RNA was converted to cDNA via RT^2 Firststrand (Qiagen). Following cDNA generation, gene expression was profiled for 89 genes using a Qiagen Calcium Signaling RT^2 Profiler PCR Array and data was evaluated utilizing the ΔΔCt. Method. The resulting fold changes in gene expression were used to determine the effects of H-FIRE treatment parameters on biological functions and complex signaling networks using Ingenuity Pathway Analysis (IPA), as previously described [44–46]. Results were normalized respectively to untreated cells. The gene list for each array and functional categories for each gene are available through the manufacturer. Ingenuity Pathways Analysis (IPA) and the manufacturer's array software (Qiagen) was used to analyze gene expression data. IPA data were ranked and evaluated based on z-score.

2.6 Statistical Analysis

Irreversible experiments were repeated 6–12 times for each condition. Reversible experiments were repeated six or more times. Discrepancies in the number of replicates between conditions were due to bubbles or other defects that may have changed the electric field distribution or prohibited a reliable measurement of ablation area. These scaffolds were excluded from analysis. Two-way ANOVA was used to test for differences in cell death area due to the different applied solutions and pulse waveforms. Tukey post-hoc comparisons were used to examine differences among treatment groups. Statistical analyses were performed with a confidence level of $\alpha = 0.05$ (JMP Pro 14). Results are shown as means ± standard deviation.

3. Results

3.1 Collagen scaffold allows testing a range of electric field magnitudes and determination of electroporation thresholds using finite element analysis

Our numerical model allows simulation and visualization of the electric field and temperature distribution in the collagen scaffold (Figure 1). Using surface integration, we can determine the area encompassed by different electric field magnitudes, enabling us to determine the electric field threshold that results in different ablation areas for each treatment. This platform provides measurements that are more relevant to in vivo treatments on tissue since the cells experience a 3D environment and are exposed to a range of electric field magnitudes. Simulating treatment resulted in a maximal temperature increase of 4.4 °C.

3.2 Adjuvant calcium increases ablation size for all conditions and is necessary to produce ablations for short pulse durations (<10 μs)

We tested a range of H-FIRE pulse durations (1, 2, 5, 10 μs) and calcium concentrations (1 mM and 5 mM) on cells seeded in collagen scaffolds to quantify cell death with and without calcium. Figure 2 shows that the ablations produced in the collagen scaffolds by calcium H-FIRE treatment are larger than NaCl controls for all pulse parameters tested. For short pulse durations (<10 μs), it seems that the cells treated with NaCl can recover from the treatment and no ablations are produced. Only in the presence of $CaCl_2$ or when longer pulse durations (>10 μs) are used, do continuous ablations form. Results suggest that the cell death response to $CaCl_2$ is dose dependent since treatments with 5 mM $CaCl_2$ result in larger ablations than those using 1 mM $CaCl_2$. As IRE and H-FIRE were delivered at different voltages, we directly compared the electric field thresholds evaluated by first quantifying ablation areas using ImageJ and a custom algorithm previously developed in MATLAB [39].

Figure 2 clearly demonstrates enhanced ablation area in response to calcium H-FIRE treatment. The increase of ablation area for 1 mM $CaCl_2$ compared to its NaCl control is nearly 2.13x for the 1–1-1 waveform, 2.79x for the 2–1-2 waveform, 5.69x for the 5–1-5 waveform, and 3.3x for the 10–1-10 waveform. For 5 mM $CaCl_2$, the 1–1-1 waveform results in a 3.47x increase in ablation area, for the 2–1-2 waveform there is a 4.37x increase, for the 5–1-5 waveform there is a 5.23x increase, and for the 10–1-10 waveform there is a 2.69x increase. As pulse duration increases, the area of ablation for $CaCl_2$ increases dramatically while for NaCl, ablation areas increase moderately. The 5–1-5 waveform

results in the largest increase of ablation area between $CaCl_2$ and NaCl treatments. For 1 mM $CaCl_2$, the 5–1-5 resulted in a 5.69x increase in ablation area compared to NaCl and for 5 mM $CaCl_2$, the 5–1-5 resulted in a 5.23x increase in ablation area. Differences seen between calcium concentrations is more pronounced for shorter pulse durations (1 and 2 μs).

3.3 Reversible electroporation zones using $CaCl_2$ are larger than NaCl controls

To investigate how $CaCl_2$ and NaCl treatments affect permeabilization of the cells, we characterized areas for reversible electroporation and their corresponding reversible electric field thresholds. Reversible electroporation thresholds for H-FIRE treatment have not been extensively characterized, making our study one of the first to quantify reversible thresholds for a range of unexplored pulse durations [47]. Figure 3 shows that both NaCl solutions had smaller reversible areas than their $CaCl_2$ counterparts, therefore the buffers used seemed to affect the extent that the cells were being permeabilized. In addition, it appeared that the difference between NaCl and $CaCl_2$ reversibly electroporated zones was similar for all waveforms. To compare the reversible zones more quantitatively, area was measured using our custom MATLAB algorithm.

Figure 3B shows that for 1 mM $CaCl_2$, the reversible zone was 1.56x larger than the 1 mM NaCl zone for the 2–1-2 waveform, 1.7x larger for the 5–1-5 waveform, and 1.42x larger for the 10–1-10 waveform. For 5 mM $CaCl_2$, the reversible zone was 1.66x larger than the 1mM NaCl zone for the 2–1-2 waveform, 1.73x for the 5–1-5 waveform, and 1.46x larger for the 10–1-10 waveform. There was no statistically significant difference between 1 mM and 5 mM treatments for the reversible case, although, after 24 hours, the 5 mM $CaCl_2$ areas are larger than the 1 mM $CaCl_2$ for shorter pulse durations suggesting that cells exposed to lower levels of calcium recover to some extent.

Figure 4 shows that reversible electroporation zones were larger than irreversible zones for all conditions tested. For the 2–1-2 waveform, reversible zones were 4.68x larger than irreversible zones for 1 mM NaCl, 3.88x for 5 mM NaCl, 2.62x for 1 mM $CaCl_2$, and 1.47x for 5 mM $CaCl_2$. For the 5–1-5 waveform reversible zones were 5.58x larger than irreversible zones for 1mM NaCl, 3.94x for 5 mM NaCl, 1.67x for 1 mM $CaCl_2$, and 1.3x for 5 mM $CaCl_2$. For the 10–1-10 waveform, reversible zones were 3.17x larger for 1 mM NaCl, 2.94x larger for 5 mM NaCl, 1.32x larger for 1 mM $CaCl_2$, and 1.59x larger for 5 mM $CaCl_2$ when compared to irreversible zones.

In Figure 4B, the difference between reversible and irreversible electroporation areas was largest for NaCl solutions. When $CaCl_2$ was used, the difference between reversible and irreversible electroporation areas decreased. As pulse duration increased, the difference between reversible and irreversible electroporation areas also decreased for all conditions.

3.4 Using adjuvant calcium in combination with a 10–1-10 H-FIRE treatment reduces the irreversible electroporation threshold to that of an IRE treatment

Using our finite element model of H-FIRE treatment in the scaffold, we were able to find the corresponding electric field thresholds for each ablation area. Table I shows that using adjuvant calcium reduces the electric field threshold in all experimental conditions. When compared to the NaCl control, 1 mM $CaCl_2$ reduces the electric field threshold 1.24x for the

1–1-1 waveform, 1.48x for the 2–2-2 waveform, 2.05x for the 5–5-5 waveform, and 2.19x for the 10–1-10 waveform. When comparing 5 mM NaCl to 5 mM $CaCl_2$, the electric field threshold is reduced 1.46x for the 1–1-1 waveform, 1.91x for the 2–1-2 waveform, 2.43x for the 5–1-5 waveform, and 1.83x for the 10–1-10 waveform. It seems the maximum effect for $CaCl_2$ is seen with 5 mM $CaCl_2$ for the 5–1-5 waveform and with 1 mM $CaCl_2$ for the 10–1-10 waveform. Using a 10–1-10 waveform with 1 mM $CaCl_2$ results in an electric field threshold of 771 ± 129 V/cm, reducing the threshold to less than half its value with NaCl (1641 ± 159 V/cm). It is important to note that 1 mM $CaCl_2$ also reduces the threshold to a level that is comparable to an IRE treatment with NaCl (698 ± 103 V/cm).

3.5 The enhanced cell death effect is unique to calcium

There are several ion channels in the plasma membrane that act to pump calcium out of the cell. One of these pumps is the Na^+-Ca^{2+} exchanger. The exchanger works to allow Na^+ to be transported into the cell while pumping Ca^{2+} out of the cell. To investigate whether NaCl would be able to aid the cells in pumping the excess Ca^{2+} out, we tested a solution that contained 1 mM of both ions. We also tested a solution of KCl to determine whether the enhanced cell death effect is unique to calcium. Figure 5 shows that the $CaCl_2$ solution and the combined solution of NaCl and $CaCl_2$ did not result in significantly different ablation sizes ($p < 0.001$), therefore, NaCl does not rescue the cells from the effect of excess Ca^{2+} and does not provide a protective mechanism (Figure 5). In addition, testing a 1 mM KCl solution did not result in statistically significant ablation size than the NaCl control, again confirming that the enhanced ablation areas were unique to calcium.

3.6 NaCl condition leads to upregulated expression of NOX1 and NOX4 while calcium upregulates expression of EIF5B

To better define the mechanisms underlying calcium-mediated cell death following H-FIRE, we profiled gene expression patterns following the treatment of cells in either $CaCl_2$ or NaCl supplemented media. Our IPA evaluation identified 4 key signaling components that were significantly impacted by the adjuvant calcium (Figure 6A). *NOX1* and *NOX4* were significantly upregulated in the NaCl treatment group compared to the downregulation observed in the $CaCl_2$ exposed cells (Figure 6A). Conversely, *EIF5B* and 60S Ribosomal Subunit signaling was significantly up-regulated in the $CaCl_2$ treatment group and significantly down-regulated in the NaCl exposed cells (Figure 6A). Both *NOX1* and *NOX4* encode NADPH oxidases that are best known for their roles in the generation of reactive oxygen species (ROS). The *EIF5B* gene encodes the Eukaryotic Translation Factor 5B that functions in translation initiation and interacts with the 60S Ribosomal Subunit. A heatmap was generated using the Average Linkage Euclidean Distance Measurement Method to better visualize the global changes in gene expression (Figure 6B). These data demonstrate the global changes in gene expression across treatment groups, with multiple differences observed between $CaCl_2$ and NaCl (Figure 6B).

Based on the significant correlation between changes in *NOX1, NOX4, EIF5B*, and the 60S ribosomal subunit signaling with NaCl and $CaCl_2$ and the diverse changes in global gene expression, IPA analysis identified a specific group of related biological functions impacted by H-FIRE treatment under the two cation conditions tested (Figure

6C). Under NaCl conditions, H-FIRE induces as significant up-regulation in *NOX1* and *NOX4* expression. This upregulation results in an increase in genes associated with NADPH Oxidase Activity (Figure 6C). However, consistent with the limited Ca^{2+} in the media, we observed gene expression changes consistent with a defect in luminal calcium signaling. Because NOX proteins require Ca^{2+} for ROS generation, these data are also consistent with the attenuation of ROS production observed in the NaCl conditions (Figure 6C). Together, these data suggest that the increase in *NOX1* and *NOX4* expression may be compensatory changes associated with the Ca^{2+} limited conditions in the NaCl buffer and likely signal attempts by the cell to generate ROS following H-FIRE treatment. Concurrently with the defect in ROS signaling, we also observed a significant decrease in EIF5B and the 60S Ribosomal Subunit signaling (Figure 6C). Consistent with these observations, IPA identified a significant decrease in pathways associated with the translation of stress related mRNA and a significant increase in signaling pathways associated with pro-survival (Figure 6C). Together, these data suggest that low Ca^{2+} conditions in the NaCl buffer provides a protective effect to minimize cell death following H-FIRE treatment.

Compared to our findings for the NaCl buffer, we observed opposite effects under the $CaCl_2$ conditions. Our results show a significant decrease in *NOX1* and *NOX4* associated signaling pathways, reduced unfolded protein response signaling, and attenuated apoptosis signaling (Figure 6C). Together, these data would suggest less cell death under these conditions. However, we also observed a significant increase in luminal calcium signaling pathways that were significantly correlated with increased cell death and a concurrent increase in signaling pathways associated with the translation of stress related mRNA (Figure 6C). These data are consistent with the increase in EIF5B and 60S Ribosomal subunit signaling that was also observed (Figure 6C). Together, the increases in these pathways resulted in an increase in necroptosis signaling, rather than apoptosis, in the $CaCl_2$ conditions following H-FIRE (Figure 6C).

4. Discussion

We have demonstrated that adjuvant calcium used in combination with H-FIRE treatment enhances ablation areas and reduces both reversible and irreversible electroporation thresholds. Pulse durations shorter than 10 μs require the use of adjuvant calcium to produce ablations larger than 5 mm^2 in vitro (Figure 2). It has been shown that shorter, bipolar pulses are less efficient at permeabilizing cells compared to longer, monopolar pulses [33,48]. Longer pulse durations cause an increase the number and/or size of pores that are created in the membrane [32,33,49], enhancing permeabilization and potentially cell death. Interestingly, the 5–1-5 waveform resulted in the largest increase of ablation area between $CaCl_2$ and NaCl treatments. The 5–1-5 waveform may be maximizing permeabilization, while minimizing cell death from irreversible electroporation in the absence of calcium. To confirm this, it was necessary to characterize the reversible ablation areas and thresholds.

When $CaCl_2$ was used, the difference between reversible and irreversible electroporation areas decreased for all waveforms (Figure 4). This result further supports our hypothesis that cells which are reversibly electroporated are driven to undergo cell death in the presence of adjuvant calcium, therefore enhancing the area of irreversible electroporation. As pulse

duration increased, the difference between reversible and irreversible electroporation areas also decreased for all conditions, suggesting that there is a transition to a higher number of cells dying. The difference between irreversible and reversible electroporation was highest for 1 mM NaCl and the 5–1-5 waveform confirming that permeabilization was maximized while cell death was minimized.

Results suggest that the cell death response to $CaCl_2$ is dose dependent for shorter pulse durations (1–5 μs). Figure 4 shows that for 5 mM $CaCl_2$, irreversible ablation areas are almost the same as reversible electroporation areas whereas for 1 mM $CaCl_2$, the irreversible is much smaller. Cells may also be able to pump lower concentrations of calcium out through the plasma membrane ATPase pump [34,50]. In addition, Ciobanu et al., demonstrated that cells electroporated in the presence of calcium (< 0.5 mM) had a lower relative fluorescence emission when exposed to PI five minutes post pulse [51] than cells that were electroporated without calcium, suggesting that low levels of calcium may aid in the resealing process [52]. The dose dependence seen in our results seems to diminish as pulse duration increases. When a 10–1-10 waveform is used, the cells may be electroporated to an extent that they cannot recover as easily and the difference in ablation area for the two calcium concentrations decreases, suggesting that there is a transition to a higher number of cells being irreversibly electroporated.

Using a 10–1-10 waveform with $CaCl_2$ decreases the cell death threshold (771 ± 129 V/cm) to a value comparable to an IRE treatment without $CaCl_2$ (698 ± 103 V/cm). This finding may allow researchers to ablate areas similar in size to traditional IRE treatments, while eliminating some of the side effects associated with IRE such as conductivity changes and dependence on tissue geometry [29]. It has been shown that decreasing pulse duration as well as the use of bipolar pulses leads to a decrease in nerve excitation [53], however elimination of muscle contractions using a 10–1-10 waveform is yet to be confirmed. In addition, using a 10 μs waveform may eliminate the need for custom built electronics to deliver the pulses, therefore reducing the complexity of pulse generator design and cost of H-FIRE treatment.

We found that $CaCl_2$ buffer lowers the electroporation threshold, causing larger reversible electroporation zones compared to NaCl buffer (Figure 3). These results match the findings of Pakhomova et al. where the authors found that cells treated in a sucrose and NaCl buffer were rescued from cell swelling and early cell death while showing increased caspase activation [54,55]. The authors hypothesized that sucrose is unable to enter pores formed during nsPEF treatment, therefore preventing cell uptake of water and subsequent rupture of the membrane. When buffer contained both $CaCl_2$ and sucrose, blebbing of the membrane was suppressed initially, followed by sudden bleb formation and massive uptake of propidium iodide leading to necrosis. Sucrose prevented cell swelling initially, but over time as more $CaCl_2$ entered the cell, existing pores either expanded or new large pores formed, allowing sucrose and PI to enter the cell. Therefore, the authors concluded that $CaCl_2$ causes cell death through a non-osmotic mechanism, although they did not specify the biological mechanism responsible. It is important to note that Pakhomova et al., used trapezoidal pulses with a duration of 300 ns whereas our pulses are square wave with longer duration (1–10 μs). It is known that pulse shape as well as duration affects pore formation

during electroporation, therefore it is possible that the dynamics of $CaCl_2$ and sucrose/NaCl uptake are different during H-FIRE treatment. However, we do see similar results in terms of $CaCl_2$ causing more permeabilization than the NaCl/sucrose solution. This similarity may suggest that pore formation during H-FIRE treatment may be similar to nsPEF treatment, however, to directly compare our results we would need to monitor cell swelling and uptake in response to H-FIRE treatment.

To investigate the differences in cellular response to $CaCl_2$ and NaCl conditions, we analyzed the regulation of calcium signaling genes. The genes chosen were pre-selected and validated by the vendor (Qiagen) to provide the broadest overview of calcium signaling pathways using a commercially available array. When the data are processed and evaluated using the vendors software and Ingenuity Pathway Analysis (also from Qiagen), the 89 genes selected are optimized to identify biological pathways and functions impacted by treatment. Our gene expression profiling identified several distinct biological functions that were significantly altered and correlated with NaCl or $CaCl_2$ environments. Under the NaCl conditions, the U251 cells were more resistant to cell death than cells treated in $CaCl_2$ conditions due in part to the downregulation of EIF5B and the eventual reduction in stress associated mRNA translation following H-FIRE in the NaCl conditions. The increase in NOX1 and NOX4 signaling should have increased cell death through increased ROS in these cells under these conditions. However, we paradoxically observed minimal ROS signaling, indeed even an attenuation (Figure 6). This is likely due to the requirement for Ca^{2+} for NOX1 signaling. In the absence of calcium, it is likely that the cell death effects associated with NOX1 and ROS production are minimized [56]. Thus, we are likely observing increased gene transcription of *NOX1* as a compensatory mechanism following H-FIRE in cells attempting to initiate ROS signaling. This is also likely associated with the increase in *NOX4* transcription. Unlike NOX1, NOX4 is constitutively active and likely upregulated at the expression level as compensation for the low calcium conditions where it can ultimately compensate for the defect in NOX1 signaling [56]. However, this delay in NOX4 signaling would be predicted to stall apoptosis in our models, as reflected in the reduced levels of cell death following H-FIRE treatment. In addition to its roles in cell death, increased expression of NOX1 also plays a role in cell proliferation where it has been demonstrated to mediate cell growth and transformation when overexpressed [57]. NOX1 regulation also targets cyclin D1 and ERK1/2 activity [58]. Thus, in addition to reduced cell death in the NaCl conditions, we are also likely observing some differences associated with increased cell proliferation and pro-survival signaling. Interestingly, Pakhomova et al. did not observe a cell sparing 24 hours after treatment with NaCl and sucrose buffer, which does not appear consistent with our findings. Perhaps the pulse parameters or cell type that we have chosen to study are responsible for this contradiction. Previous research has shown that the mechanism of cell death may differ between cell types as well as pulse strength and duration [47,59].

Conversely, the U251 cells were more sensitive to H-FIRE treatment in the $CaCl_2$ conditions than they were in the NaCl conditions. This is due, in part, to the upregulation of EIF5B and the eventual induction of necroptosis. EIF5B represents a regulatory node in cancer cells, whereby under some conditions increased gene expression is associated with cell evasion of apoptosis by promoting the translation of pro-survival proteins, while under other

conditions overexpression promotes cell cycle defects resulting in cell death in response to stress [60,61]. Our data is consistent with the later findings, whereby in conditions of calcium enrichment followed by cellular stress and damage associated with H-FIRE, we observe significantly increased cell death. Likewise, the anti-apoptotic functions of EIF5B, associated with the upregulation of *XIAP* and *BCL-XL*, may function as a significant driver of the increased necroptosis signaling as the predominate form of early cell death in the U251 cells following H-FIRE in the $CaCl_2$ conditions (Figure 6). Finally, it should be noted that dysregulated increases in intracellular calcium can promote cell death through necrosis following cellular damage and/or stress [62]. One limitation of our study is that we analyzed gene expression of cells that were exposed to a range of electric field magnitudes which may be experiencing differential gene expression. To accommodate for this limitation, we normalized our results to sham controls to observe general trends. However, in future work it may be useful to investigate gene expression in response to a uniform electric field magnitude. Such investigations would allow for precise characterization of cell response for different electric field strengths. Our results can be used to inform future studies as to which electric field magnitudes may be of interest for future investigations into H-FIRE treatment with and without calcium.

While the exact mechanism distinguishing cell death for NaCl and $CaCl_2$ still needs further investigation, several molecular dynamics studies have shown that calcium interacts with and can even bind to the lipid head groups of the membrane [63]. These interactions may influence pore formation, pore lifetime, and pore resealing [63,64]. It has also recently been demonstrated that lipid composition varies between cell type and can further influence pore formation and interaction of ions with the membrane [65]. Furthermore, previous studies have shown that an excess of intracellular calcium may activate proteases and phospholipases which further contribute to the lifetime of pores and exacerbate membrane damage, subsequently preventing resealing of the membrane [66].

5. Conclusion

We have demonstrated successful enhancement of H-FIRE ablations using adjuvant calcium. Utilizing a 10–1-10 H-FIRE waveform with 1 mM $CaCl_2$ reduces the irreversible electroporation threshold to a value comparable to standard IRE treatments without calcium, therefore enhancing the efficacy of H-FIRE without increasing the applied voltage. This finding may potentially allow clinicians to use commercially available generators instead of custom-made generators for treatment, simplifying translation to the clinic. We have also uncovered several distinct biological functions that were significantly altered and correlated with NaCl or $CaCl_2$ environments.

Calcium electroporation has recently been investigated in several clinical trials for cutaneous metastases, colon as well as head and neck cancer [36,67,68]. We envision using calcium H-FIRE treatment in vivo in a similar fashion to enhance ablation size by injecting calcium chloride directly into the tumor and delivering H-FIRE pulses through needle electrodes inserted into the tumor. However, translating to the clinic still presents challenges such as optimizing $CaCl_2$ concentration as well as injection volume as to avoid necrosis of surrounding tissue and hypercalcemia.

Following our observation that sucrose and NaCl may prevent cell death, we also envision injecting a buffer that contains sucrose and lacks calcium to control electroporation treatments in vivo, therefore preserving tissue that is outside of the desired ablation zone. This sucrose buffer could be injected into blood vessels near tumors prior to treatment to prevent electroporation of the endothelial cells in the vessel. Spatial control over ablations and sparing of blood vessels may be beneficial for treatments such as blood-brain barrier disruption. Electrodes may be designed to inject $CaCl_2$ into the tumor during treatment while also delivering NaCl and sucrose buffer on the tumor borders to protect surrounding tissue. Venofer is an Iron Sucrose solution (300 mg/ml sucrose w/v) that is administered intravenously and utilized to treat anemia. Side effects are relatively minor and include muscle cramps, nausea, vomiting, and dizziness. Most side effects are associated with the speed of administration. However, it would be reasonable to utilize something like Venofer to increase sucrose concentrations as supported by the data provided here.

In addition, these results suggest that adding calcium to electroporation buffers prior to gene transfection procedures may enhance permeabilization and therefore cell uptake [35]. Our study is the first to demonstrate enhancement of H-FIRE ablations using adjuvant calcium, in addition to identifying key genes and signaling pathways responsible for differences in cell death with and without calcium.

Supplementary Material

Refer to Web version on PubMed Central for supplementary material.

Funding:

This work was supported by the Virginia-Maryland College of Veterinary Medicine (I.C.A.), the Virginia Tech Institute for Critical Technology and Applied Science Center for Engineered Health (I.C.A.), the Virginia Biosciences Health Research Corporation (VBHRC) Catalyst (R.V.D.), and the National Institutes of Health R01CA213423 (R.V.D. and S.S.V.), P01CA207206 (R.V.D. and S.S.V). The content is solely the responsibility of the authors and does not necessarily represent the official views of the NIH or any other funding agency.

References

[1]. Martin RCG, Kwon D, Chalikonda S, Sellers M, Kotz E, Scoggins C, McMasters KM, Watkins K, Treatment of 200 Locally Advanced (Stage III) Pancreatic Adenocarcinoma Patients With Irreversible Electroporation, Ann. Surg 262 (2015) 486–494. doi:10.1097/SLA.0000000000001441. [PubMed: 26258317]

[2]. Sugimoto K, Moriyasu F, Kobayashi Y, Saito K, Takeuchi H, Ogawa S, Ando M, Sano T, Mori T, Furuichi Y, Nakamura I, Irreversible electroporation for nonthermal tumor ablation in patients with hepatocellular carcinoma: initial clinical experience in Japan, Jpn. J. Radiol 33 (2015) 424–432. doi:10.1007/s11604-015-0442-1. [PubMed: 26032929]

[3]. Paiella S, Butturini G, Frigerio I, Salvia R, Armatura G, Bacchion M, Fontana M, D"Onofrio M, Martone E, Bassi C, Safety and Feasibility of Irreversible Electroporation (IRE) in Patients with Locally Advanced Pancreatic Cancer: Results of a Prospective Study, Dig. Surg 32 (2015) 90–97. doi:10.1159/000375323. [PubMed: 25765775]

[4]. Scheffer HJ, Vroomen LGPH, de Jong MC, Melenhorst MCAM, Zonderhuis BM, Daams F, Vogel JA, Besselink MGH, van Kuijk C, Witvliet J, de van der Schueren MAE, de Gruijl TD, Stam AGM, van den Tol PMP, van Delft F, Kazemier G, Meijerink MR, Ablation of Locally Advanced Pancreatic Cancer with Percutaneous Irreversible Electroporation: Results of the Phase

I/II PANFIRE Study, Radiology. 282 (2017) 585–597. doi:10.1148/radiol.2016152835. [PubMed: 27604035]

[5]. Garcia PA, Pancotto T, Rossmeisl JH, Henao-Guerrero N, Gustafson NR, Daniel GB, Robertson JL, Ellis TL, V Davalos R, Non-thermal irreversible electroporation (N-TIRE) and adjuvant fractionated radiotherapeutic multimodal therapy for intracranial malignant glioma in a canine patient., Technol. Cancer Res. Treat 10 (2011) 73–83. doi:10.1111/j.1939-1676.2011.00862.x. [PubMed: 21214290]

[6]. Rossmeisl JH, Garcia PA, Roberston JL, Ellis TL, Davalos RV, Pathology of non-thermal irreversible electroporation (N-TIRE)-induced ablation of the canine brain, J. Vet. Sci 14 (2013) 433–440. doi:10.4142/jvs.2013.14.4.433. [PubMed: 23820168]

[7]. Garcia PA, Rossmeisl JH, Neal RE, Ellis TL, Olson JD, Henao-Guerrero N, Robertson J, Davalos RV, Intracranial nonthermal irreversible electroporation: In vivo analysis, J. Membr. Biol 236 (2010) 127–136. doi:10.1007/s00232-010-9284-z. [PubMed: 20668843]

[8]. Ellis TL, Garcia PA, Rossmeisl JH, Henao-Guerrero N, Robertson J, V Davalos R, Nonthermal irreversible electroporation for intracranial surgical applications. Laboratory investigation., J. Neurosurg 114 (2011) 681–688. doi:10.3171/2010.5.JNS091448. [PubMed: 20560725]

[9]. Glaser RW, Leikin SL, Chernomordik LV, Pastushenko VF, Sokirko AI, Reversible electrical breakdown of lipid bilayers: formation and evolution of pores, BBA - Biomembr. 940 (1988) 275–287. doi:10.1016/0005-2736(88)90202-7.

[10]. Abidor IG, Arakelyan VB, Chernomordik LV, Chizmadzhev YA, Pastushenko VF, Tarasevich MP, Electric breakdown of bilayer lipid membranes. I. The main experimental facts and their qualitative discussion, J. Electroanal. Chem 104 (1979) 37–52. doi:10.1016/S0022-0728(79)81006-2.

[11]. Hristov K, Mangalanathan U, Casciola M, Pakhomova ON, Pakhomov AG, Expression of voltage-gated calcium channels augments cell susceptibility to membrane disruption by nanosecond pulsed electric field, Biochim. Biophys. Acta - Biomembr 1860 (2018) 2175–2183. doi:10.1016/j.bbamem.2018.08.017. [PubMed: 30409513]

[12]. Suzuki K, Tsunekawa Y, Hernandez-Benitez R, Wu J, Zhu J, Kim EJ, Hatanaka F, Yamamoto M, Araoka T, Li Z, Kurita M, Hishida T, Li M, Aizawa E, Guo S, Chen S, Goebl A, Soligalla RD, Qu J, Jiang T, Fu X, Jafari M, Esteban CR, Berggren WT, Lajara J, Nuñez-Delicado E, Guillen P, Campistol JM, Matsuzaki F, Liu G-H, Magistretti P, Zhang K, Callaway EM, Zhang K, Belmonte JCI, In vivo genome editing via CRISPR/Cas9 mediated homology-independent targeted integration, Nature. 540 (2016) 144–149. doi:10.1038/nature20565. [PubMed: 27851729]

[13]. Dower WJ, Miller JF, Ragsdale CW, High efficiency transformation of E.coli by high voltage electroporation, Nucleic Acids Res. 16 (1988) 6127–6145. doi:10.1093/nar/16.13.6127. [PubMed: 3041370]

[14]. Gothelf A, Mir LM, Gehl J, Electrochemotherapy: Results of cancer treatment using enhanced delivery of bleomycin by electroporation, Cancer Treat. Rev 29 (2003) 371–387. doi:10.1016/S0305-7372(03)00073-2. [PubMed: 12972356]

[15]. Linnert M, Agerholm-Larsen B, Mahmood F, Iversen HK, Gehl J, Treatment of Brain Tumors: Electrochemotherapy, in: Springer Netherlands, 2014: pp. 247–259. http://link.springer.com/10.1007/978-94-007-7217-5_22 (accessed July 6, 2016).

[16]. Salford LG, Persson BRR, Brun A, Ceberg CP, Kongstad PC, Mir LM, A New Brain Tumor Therapy Combining Bleomycin with in Vivo Electropermeabilization, Biochem. Biophys. Res. Commun 194 (1993) 938–943. doi:10.1006/bbrc.1993.1911. [PubMed: 7688229]

[17]. Sersa G, Teissie J, Cemazar M, Signori E, Kamensek U, Marshall G, Miklavcic D, Electrochemotherapy of tumors as in situ vaccination boosted by immunogene electrotransfer, Cancer Immunol. Immunother 64 (2015) 1315–1327. doi:10.1007/s00262-015-1724-2. [PubMed: 26067277]

[18]. Davalos RV, Rubinsky B, Mir LM, Theoretical analysis of the thermal effects during in vivo tissue electroporation, Bioelectrochemistry. 61 (2003) 99–107. doi:10.1016/j.bioelechem.2003.07.001. [PubMed: 14642915]

[19]. Li W, Fan Q, Ji Z, Qiu X, Li Z, The Effects of Irreversible Electroporation (IRE) on Nerves, PLoS One. 6 (2011) e18831. doi:10.1371/journal.pone.0018831.

[20]. Rossmeisl JH, Garcia PA, Pancotto TE, Robertson JL, Henao-Guerrero N, Neal RE, Ellis TL, Davalos RV, Safety and feasibility of the NanoKnife system for irreversible electroporation ablative treatment of canine spontaneous intracranial gliomas, J. Neurosurg 123 (2015) 1008–1025. doi:10.3171/2014.12.JNS141768. [PubMed: 26140483]

[21]. Martin RCG, McFarland K, Ellis S, Velanovich V, Irreversible electroporation therapy in the management of locally advanced pancreatic adenocarcinoma, J. Am. Coll. Surg 215 (2012) 361–369. doi:10.1016/j.jamcollsurg.2012.05.021. [PubMed: 22726894]

[22]. Ball C, Thomson KR, Kavnoudias H, Irreversible electroporation: a new challenge in "out of operating theater" anesthesia., Anesth. Analg 110 (2010) 1305–9. doi:10.1213/ANE.0b013e3181d27b30. [PubMed: 20142349]

[23]. Thomson KR, Cheung W, Ellis SJ, Federman D, Kavnoudias H, Loader-Oliver D, Roberts S, Evans P, Ball C, Haydon A, Investigation of the Safety of Irreversible Electroporation in Humans, J. Vasc. Interv. Radiol 22 (2011) 611–621. doi:10.1016/J.JVIR.2010.12.014. [PubMed: 21439847]

[24]. Arena CB, Sano MB, Rossmeisl JH, Caldwell JL, a Garcia P, Rylander MN, V Davalos R, High-frequency irreversible electroporation (H-FIRE) for non-thermal ablation without muscle contraction., Biomed. Eng. Online 10 (2011) 102. doi:10.1186/1475-925X-10-102. [PubMed: 22104372]

[25]. Pavlin M, Pavselj N, Miklavcic D, Dependence of induced transmembrane potential on cell density, arrangement, and cell position inside a cell system., IEEE Trans. Biomed. Eng 49 (2002) 605–12. doi:10.1109/TBME.2002.1001975. [PubMed: 12046706]

[26]. Murovec T, Sweeney DC, Latouche E, Davalos RV, Brosseau C, Modeling of Transmembrane Potential in Realistic Multicellular Structures before Electroporation, 111 (2016) 2286–2295. https://www.sbes.vt.edu/davalos/pdf/1-s2.0-S0006349516309328main.pdf (accessed January 25, 2018).

[27]. Pucihar G, Kotnik T, Valič B, Miklavčič D, Numerical determination of transmembrane voltage induced on irregularly shaped cells, Ann. Biomed. Eng 34 (2006) 642–652. doi:10.1007/s10439-005-9076-2. [PubMed: 16547608]

[28]. Bhonsle S, Lorenzo M, Safaai-Jazi A, Davalos RV, Characterization of Nonlinearity and Dispersion in Tissue Impedance during High Frequency Electroporation, IEEE Trans. Biomed. Eng (2017) 1–1. doi:10.1109/TBME.2017.2787038.

[29]. Zhao Y, Bhonsle S, Dong S, Lv Y, Liu H, Safaai-Jazi A, Davalos RV, Yao C, Characterization of conductivity changes during high-frequency irreversible electroporation for treatment planning, IEEE Trans. Biomed. Eng 65 (2018) 1810–1819. doi:10.1109/TBME.2017.2778101. [PubMed: 29989932]

[30]. Bhonsle SP, Arena CB, Sweeney DC, V Davalos R, Mitigation of impedance changes due to electroporation therapy using bursts of high-frequency bipolar pulses., Biomed. Eng. Online. 14 Suppl 3 (2015) S3. doi:10.1186/1475-925X-14-S3-S3.

[31]. Arena CB, Sano MB, Rylander MN, V Davalos R, Theoretical considerations of tissue electroporation with high-frequency bipolar pulses., IEEE Trans. Biomed. Eng 58 (2011) 1474–82. doi:10.1109/TBME.2010.2102021. [PubMed: 21189230]

[32]. Sano MB, Arena CB, DeWitt MR, Saur D, Davalos RV, In-vitro bipolar nano- and microsecond electro-pulse bursts for irreversible electroporation therapies, Bioelectrochemistry. 100 (2014) 69–79. doi:10.1016/J.BIOELECHEM.2014.07.010. [PubMed: 25131187]

[33]. Sweeney DC, Reberšek M, Dermol J, Rems L, Miklavčič D, Davalos RV, Quantification of cell membrane permeability induced by monopolar and high-frequency bipolar bursts of electrical pulses, Biochim. Biophys. Acta - Biomembr 1858 (2016) 2689–2698. doi:10.1016/j.bbamem.2016.06.024.

[34]. Frandsen SK, Gissel H, Hojman P, Tramm T, Eriksen J, Gehl J, Direct therapeutic applications of calcium electroporation to effectively induce tumor necrosis., Cancer Res. 72 (2012) 1336–41. doi:10.1158/0008-5472.CAN-11-3782. [PubMed: 22282658]

[35]. Frandsen SK, Gissel H, Hojman P, Eriksen J, Gehl J, Calcium electroporation in three cell lines: A comparison of bleomycin and calcium, calcium compounds, and pulsing conditions, Biochim. Biophys. Acta - Gen. Subj 1840 (2014) 1204–1208. doi:10.1016/j.bbagen.2013.12.003.

[36]. Falk H, Matthiessen LW, Wooler G, Gehl J, Calcium electroporation for treatment of cutaneous metastases; a randomized double-blinded phase II study, comparing the effect of calcium electroporation with electrochemotherapy, Acta Oncol. (Madr) (2017) 1–9. doi:10.1080/0284186X.2017.1355109.

[37]. Hansen EL, Sozer EB, Romeo S, Frandsen SK, Vernier PT, Gehl J, Dose-Dependent ATP Depletion and Cancer Cell Death following Calcium Electroporation, Relative Effect of Calcium Concentration and Electric Field Strength, PLoS One. 10 (2015) e0122973. 10.1371/journal.pone.0122973 (accessed June 30, 2016).

[38]. Frandsen SK, Krüger MB, Mangalanathan UM, Tramm T, Mahmood F, Novak I, Gehl J, Normal and malignant cells exhibit differential responses to calcium electroporation, Cancer Res. 77 (2017) 4389–4401. doi:10.1158/0008-5472.CAN-16-1611. [PubMed: 28760856]

[39]. Wasson EMEM, Ivey JWJW, Verbridge SSS, V Davalos RVR, The Feasibility of Enhancing Susceptibility of Glioblastoma Cells to IRE Using a Calcium Adjuvant, Ann. Biomed. Eng 45 (2017) 2535–2547. doi:10.1007/s10439-017-1905-6. [PubMed: 28849278]

[40]. Melikov KC, Frolov VA, Shcherbakov A, Samsonov AV, Chizmadzhev YA, Chernomordik LV, Voltage-Induced Nonconductive Pre-Pores and Metastable Single Pores in Unmodified Planar Lipid Bilayer, Biophys. J 80 (2001) 1829–1836. doi:10.1016/S0006-3495(01)76153-X. [PubMed: 11259296]

[41]. Koronkiewicz S, Kalinowski S, Bryl K, Programmable chronopotentiometry as a tool for the study of electroporation and resealing of pores in bilayer lipid membranes, Biochim. Biophys. Acta - Biomembr 1561 (2002) 222–229. doi:10.1016/S0005-2736(02)00347-4.

[42]. Arena CB, Szot CS, Garcia PA, Rylander MN, Davalos RV, A three-dimensional in vitro tumor platform for modeling therapeutic irreversible electroporation, Biophys. J 103 (2012) 2033–2042. doi:10.1016/j.bpj.2012.09.017. [PubMed: 23199931]

[43]. Ivey JW, Latouche EL, Sano MB, Rossmeisl JH, Davalos RV, Verbridge SS, Targeted cellular ablation based on the morphology of malignant cells, Sci. Rep 5 (2015) 17157. doi:10.1038/srep17157. [PubMed: 26596248]

[44]. Eden K, Rothschild DE, McDaniel DK, Heid B, Allen IC, Noncanonical NF-κB signaling and the essential kinase NIK modulate crucial features associated with eosinophilic esophagitis pathogenesis., Dis. Model. Mech 10 (2017) 1517–1527. doi:10.1242/dmm.030767. [PubMed: 29259025]

[45]. Theus MH, Brickler T, Meza AL, Coutermarsh-Ott S, Hazy A, Gris D, Allen IC, Loss of NLRX1 Exacerbates Neural Tissue Damage and NF-κB Signaling following Brain Injury., J. Immunol 199 (2017) 3547–3558. doi:10.4049/jimmunol.1700251. [PubMed: 28993512]

[46]. Allen IC, Moore CB, Schneider M, Lei Y, Davis BK, Scull MA, Gris D, Roney KE, Zimmermann AG, Bowzard JB, Ranjan P, Monroe KM, Pickles RJ, Sambhara S, Ting JPY, NLRX1 Protein Attenuates Inflammatory Responses to Infection by Interfering with the RIG-I-MAVS and TRAF6-NF-κB Signaling Pathways, Immunity. 34 (2011) 854–865. doi:10.1016/J.IMMUNI.2011.03.026. [PubMed: 21703540]

[47]. Weaver JC, Smith KC, Esser AT, Son RS, Gowrishankar TR, A brief overview of electroporation pulse strength-duration space: a region where additional intracellular effects are expected., Bioelectrochemistry. 87 (2012) 236–43. doi:10.1016/j.bioelechem.2012.02.007. [PubMed: 22475953]

[48]. Ibey BL, Ullery JC, Pakhomova ON, Roth CC, Semenov I, Beier HT, Tarango M, Xiao S, Schoenbach KH, Pakhomov AG, Bipolar nanosecond electric pulses are less efficient at electropermeabilization and killing cells than monopolar pulses., Biochem. Biophys. Res. Commun 443 (2014) 568–73. doi:10.1016/j.bbrc.2013.12.004. [PubMed: 24332942]

[49]. Delemotte L, Tarek M, Molecular Dynamics Simulations of Lipid Membrane Electroporation, J. Membr. Biol 245 (2012) 531–543. doi:10.1007/s00232-012-9434-6. [PubMed: 22644388]

[50]. Lee RC, Canaday DJ, Hammer SM, Transient and stable ionic permeabilization of isolated skeletal muscle cells after electrical shock, J. Burn Care Rehabil 14 (1993) 528–40. doi:10.1097/00004630-199309000-00007. [PubMed: 8245107]

[51]. Ciobanu F, Golzio M, Kovacs E, Teissié J, Control by Low Levels of Calcium of Mammalian Cell Membrane Electropermeabilization, J. Membr. Biol 251 (2018) 221–228. doi:10.1007/s00232-017-9981-y. [PubMed: 28823021]

[52]. Dermol J, Pakhomova ON, Pakhomov AG, Miklavčič D, Cell Electrosensitization Exists Only in Certain Electroporation Buffers, PLoS One. 11 (2016) e0159434. doi:10.1371/journal.pone.0159434.

[53]. Mercadal B, Arena CB, V Davalos R, Ivorra A, Avoiding nerve stimulation in irreversible electroporation: a numerical modeling study, Phys. Med. Biol. Accept. Manuscr (2017). doi:10.1088/1361-6560/aa8c53.

[54]. Nesin OM, Pakhomova ON, Xiao S, Pakhomov AG, Manipulation of cell volume and membrane pore comparison following single cell permeabilization with 60- and 600-ns electric pulses, Biochim. Biophys. Acta - Biomembr 1808 (2011) 792–801. doi:10.1016/J.BBAMEM.2010.12.012.

[55]. Pakhomova ON, Gregory B, Semenov I, Pakhomov AG, Calcium-mediated pore expansion and cell death following nanoelectroporation, BBA - Biomembr. 1838 (2014) 2547–2554. doi:10.1016/j.bbamem.2014.06.015.

[56]. Brown DI, Griendling KK, Nox proteins in signal transduction., Free Radic. Biol. Med 47 (2009) 1239–53. doi:10.1016/j.freeradbiomed.2009.07.023. [PubMed: 19628035]

[57]. Arnold RS, Shi J, Murad E, Whalen AM, Sun CQ, Polavarapu R, Parthasarathy S, Petros JA, Lambeth JD, Hydrogen peroxide mediates the cell growth and transformation caused by the mitogenic oxidase Nox1., Proc. Natl. Acad. Sci. U. S. A 98 (2001) 5550–5. doi:10.1073/pnas.101505898. [PubMed: 11331784]

[58]. Burch PM, Heintz NH, Redox Regulation of Cell-Cycle Re-entry: Cyclin D1 as a Primary Target for the Mitogenic Effects of Reactive Oxygen and Nitrogen Species, Antioxid. Redox Signal 7 (2005) 741–751. doi:10.1089/ars.2005.7.741. [PubMed: 15890020]

[59]. Morotomi-Yano K, Akiyama H, Yano K, Different involvement of extracellular calcium in two modes of cell death induced by nanosecond pulsed electric fields, Arch. Biochem. Biophys 555–556 (2014) 47–54. doi:10.1016/J.ABB.2014.05.020.

[60]. Ross JA, Vanden Dungen K, Bressler KR, Fredriksen M, Khandige Sharma D, Balasingam N, Thakor N, Eukaryotic initiation factor 5B (eIF5B) provides a critical cell survival switch to glioblastoma cells via regulation of apoptosis, Cell Death Dis. 10 (2019) 57. doi:10.1038/s41419-018-1283-5. [PubMed: 30670698]

[61]. Lee S, Truesdell SS, Bukhari SIA, Lee JH, LeTonqueze O, Vasudevan S, Upregulation of eIF5B controls cell-cycle arrest and specific developmental stages., Proc. Natl. Acad. Sci. U. S. A 111 (2014) E4315–22. doi:10.1073/pnas.1320477111. [PubMed: 25261552]

[62]. Pinton P, Giorgi C, Siviero R, Zecchini E, Rizzuto R, Calcium and apoptosis: ER-mitochondria Ca2+ transfer in the control of apoptosis, Oncogene. 27 (2008) 6407–6418. doi:10.1038/onc.2008.308. [PubMed: 18955969]

[63]. Levine ZA, Vernier PT, Calcium and Phosphatidylserine Inhibit Lipid Electropore Formation and Reduce Pore Lifetime, J. Membr. Biol 245 (2012) 599–610. doi:10.1007/s00232-012-9471-1. [PubMed: 22815071]

[64]. Sridhara V, Joshi RP, Evaluations of a mechanistic hypothesis for the influence of extracellular ions on electroporation due to high-intensity, nanosecond pulsing, Biochim. Biophys. Acta - Biomembr 1838 (2014) 1793–1800. doi:10.1016/J.BBAMEM.2014.03.010.

[65]. Hoejholt KL, Mužić T, Jensen SD, Dalgaard LT, Bilgin M, Nylandsted J, Heimburg T, Frandsen SK, Gehl J, Calcium electroporation and electrochemotherapy for cancer treatment: Importance of cell membrane composition investigated by lipidomics, calorimetry and in vitro efficacy, Sci. Rep 9 (2019) 4758. doi:10.1038/s41598-019-41188-z. [PubMed: 30894594]

[66]. Gissel H, Clausen T, Ca2+ uptake and cellular integrity in rat EDL muscle exposed to electrostimulation, electroporation, or A23187, Am. J. Physiol. - Regul. Integr. Comp. Physiol 285 (2003). http://ajpregu.physiology.org/content/285/1/R132 (accessed July 9, 2017).

[67]. Broholm M, Stigaard T, Bulut M, Vogelsang R, Gögenur I, Gehl J, Calcium electroporation for the treatment of colorectal cancer calcium endove – preliminary results, Eur. J. Surg. Oncol 45 (2019) e119. doi:10.1016/j.ejso.2018.10.409.

[68]. Plaschke CC, Gehl J, Johannesen HH, Fischer BM, Kjaer A, Lomholt AF, Wessel I, Calcium electroporation for recurrent head and neck cancer: A clinical phase I study, Laryngoscope Investig. Otolaryngol 4 (2019) 49–56. doi:10.1002/lio2.233.

Highlights:

- $CaCl_2$ enhances ablation volume for H-FIRE treatment of varying pulse widths
- $CaCl_2$ enhances permeabilization of cells compared to a NaCl control
- $CaCl_2$ upregulates expression of eIFB5 and 60s ribosomal subunit genes
- $CaCl_2$ treatment leads to increased signaling in pathways that may cause necroptosis
- Treatment without $CaCl_2$ upregulates expression of NOX1/4 genes
- Treatment without $CaCl_2$ leads to an increase in pro survival signaling

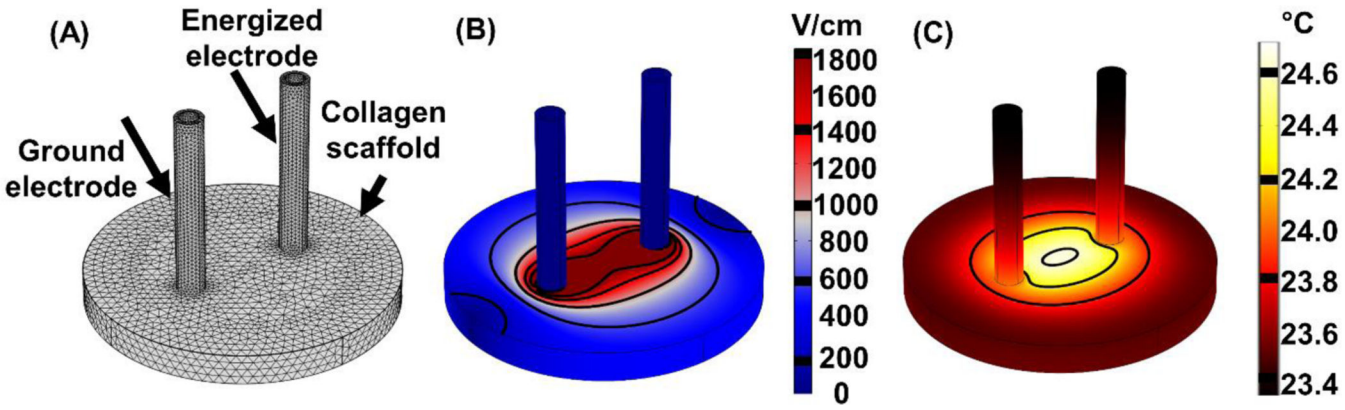

Figure 1: Simulating H-FIRE treatments using the finite element method allows us to determine the electric field and temperature distribution in the collagen scaffold.

(A) The mesh was refined until there was < 1% change in electric field and temperature values along a cutline between the electrodes. The mesh consisted of 102,615 total elements. **(B)** Solving for the electric field distribution and quantifying area of electroporation allows us to determine the electric field threshold for each treatment. 800 V was applied with an electrode spacing of 4 mm (center-to-center). **(C)** Using the highest conductivity buffer (σ = 0.131 S/m) in the simulation led to a predicted increase in temperature of 4.4 °C in the collagen scaffold.

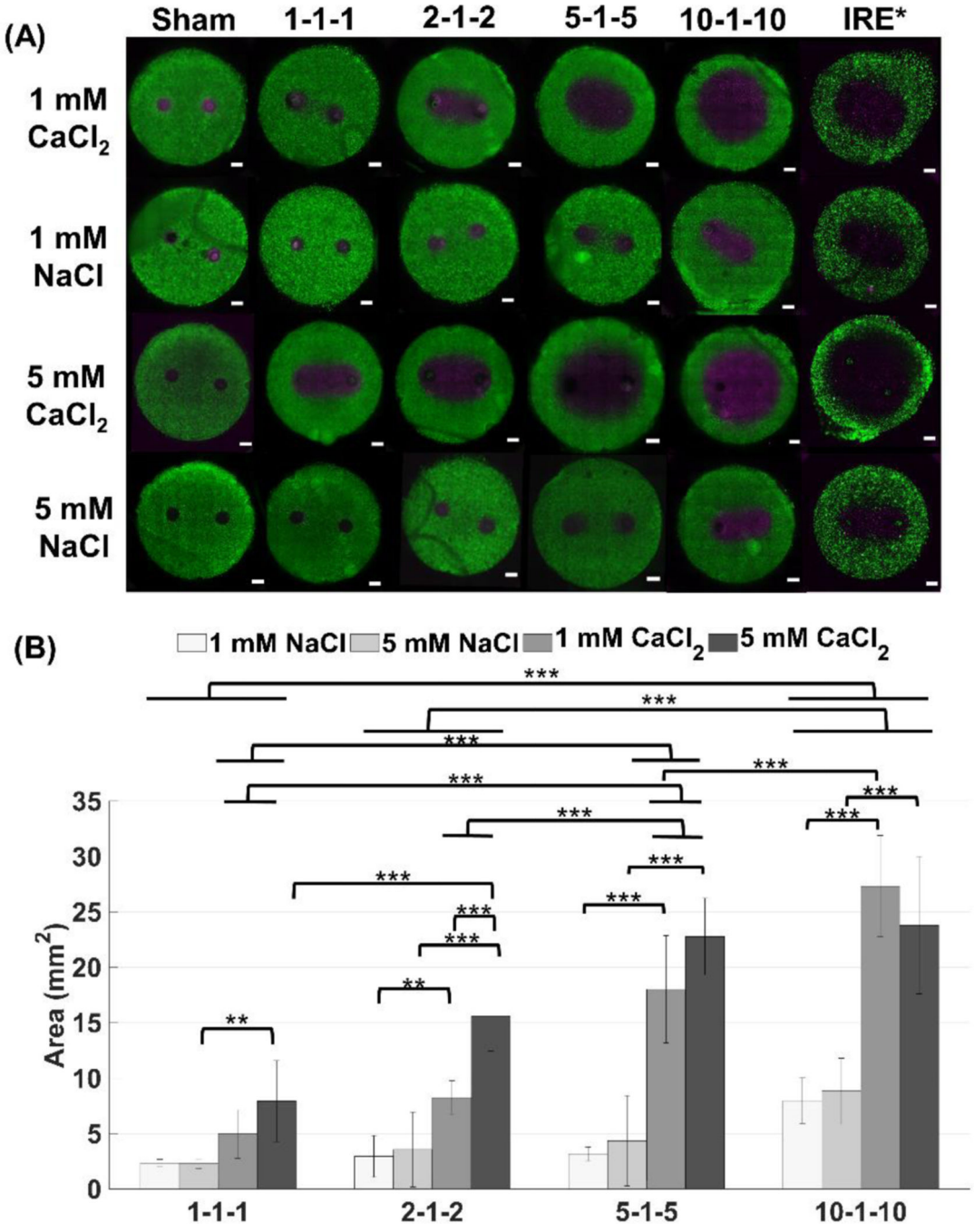

Figure 2: Ablation areas for $CaCl_2$ are significantly larger than ablations for NaCl for all pulse durations. Pulse durations below 10 μs, need $CaCl_2$ to produce an ablation larger than 5 mm^2 (*p < 0.001, **p < 0.05, scale bar 1mm).**

(A) In vitro collagen scaffolds consisted of 5 mg/mL rat tail collagen type I and U251 malignant glioma cells (1×10^6 cells/mL). Electrodes were spaced 4 mm apart (center-to-center). For IRE treatments, 80, 100 μs pulses were delivered at 450 V and 1 Hz frequency. For H-FIRE treatments, 80 bursts of various pulse durations were delivered at 800 V at a frequency of 1 burst/second for a total on time of 100 μs. Live cells are stained with calcein AM (green) while dead and/or membrane compromised cells are stained with propidium

iodide (magenta). Propidium iodide stains cells red, but the images are shown in magenta for visualization purposes ($n \geq 6$ for all conditions). **(B)** Ablations were measured using a custom algorithm developed in MATLAB and ImageJ. The total area of the scaffold was 78.54 mm^2 (10 mm diameter) with a thickness of 1 mm. Results are shown as mean ± std. *IRE data was taken from a previous study (Wasson et al., 2017) [39].

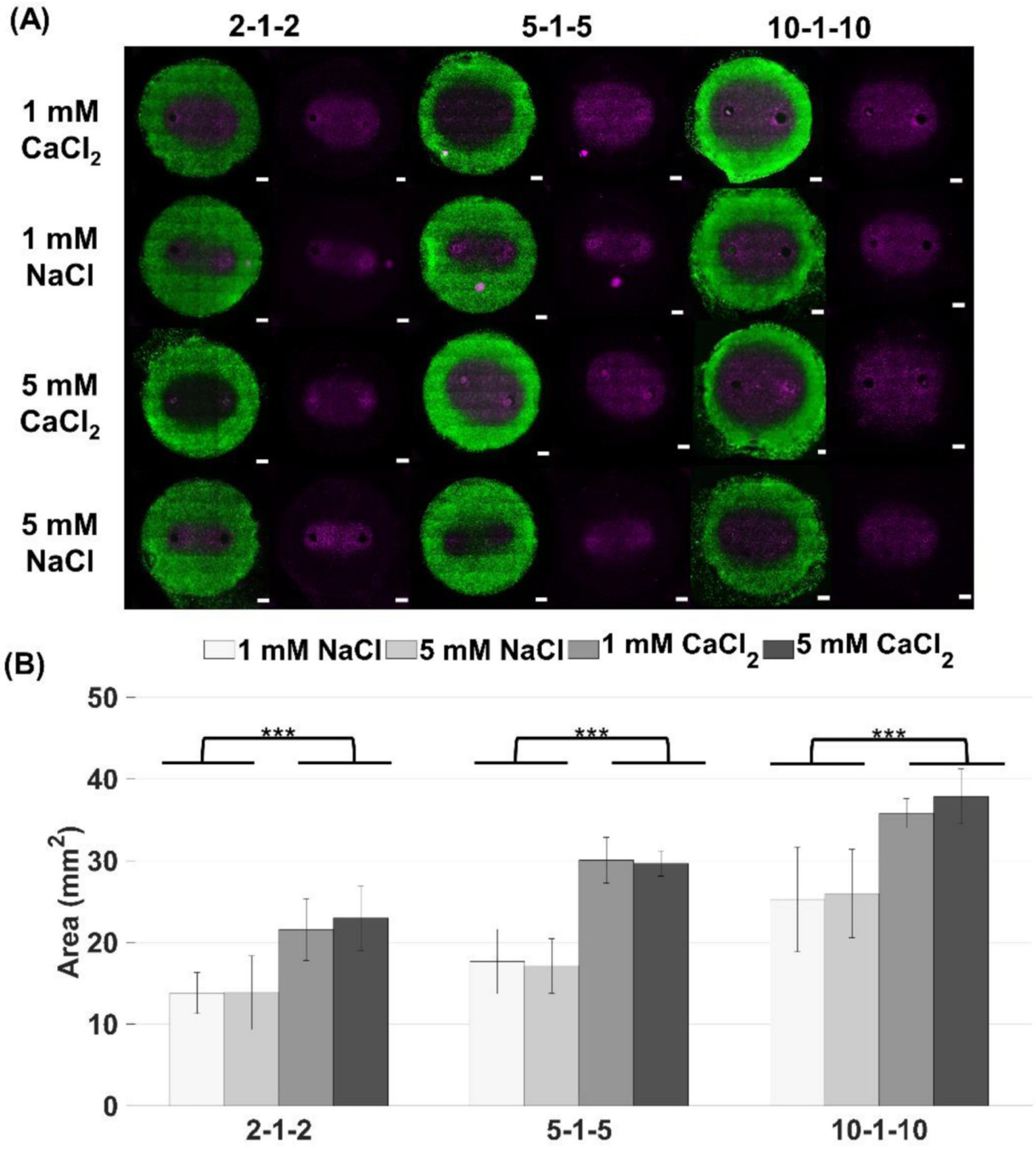

Figure 3: Reversible electroporation areas show that the NaCl buffer produces a smaller affected area than the $CaCl_2$ buffer indicating the cells are electroporated to a lesser extent. The NaCl buffer may provide protection against cell death whereas the $CaCl_2$ solution does not (* $p < 0.001$).**

(A) The image on the left of each panel shows the both the unpermeabilized (green) and permeabilized (violet) regions of cells while the image on the right (violet alone) shows permeabilized cells alone. In vitro collagen scaffolds consisted of 5 mg/mL rat tail collagen type I and U251 malignant gliomas (1×10^6 cells/mL). H-FIRE treatments consisted of delivering 80 bursts of pulses with various durations at 800 V and a frequency of 1 burst/

second for a total on time of 100 μs. The total area of the scaffold was 78.54 mm^2 (10 mm diameter) with a thickness of 1 mm. **(B)** Reversible electroporation areas were measured using Image J and a custom algorithm developed in MATLAB. Electrodes were spaced 4 mm apart (center-to-center). Results are shown as mean ± std ($n \geq 6$ for all conditions).

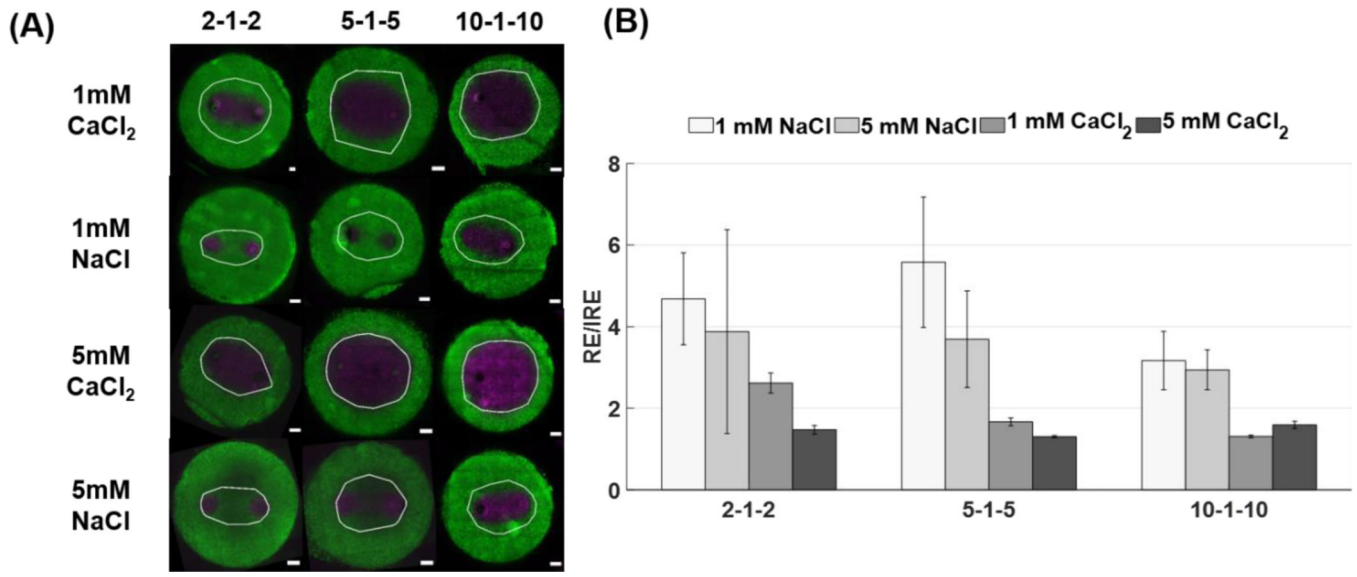

Figure 4: $CaCl_2$ reduces the difference between reversible and irreversible electroporation areas.
(A) Reversible electroporation zones are overlaid (white) onto irreversible ablation images to demonstrate the effect calcium has on enhancing the ablation margin. In vitro collagen scaffolds consisted of 5 mg/mL rat tail collagen type I and U251 malignant gliomas (1×10^6 cells/mL). H-FIRE treatments consisted of delivering 80 bursts of pulses with various durations at 800 V and a frequency of 1 burst/second for a total on time of 100 μs. The total area of the scaffold was 78.54 mm^2 (10 mm diameter) with a thickness of 1 mm.
(B) The ratio of reversible electroporation (RE) to irreversible ablation areas (IRE) and the propagated uncertainty were calculated. Results are shown as mean ± std.

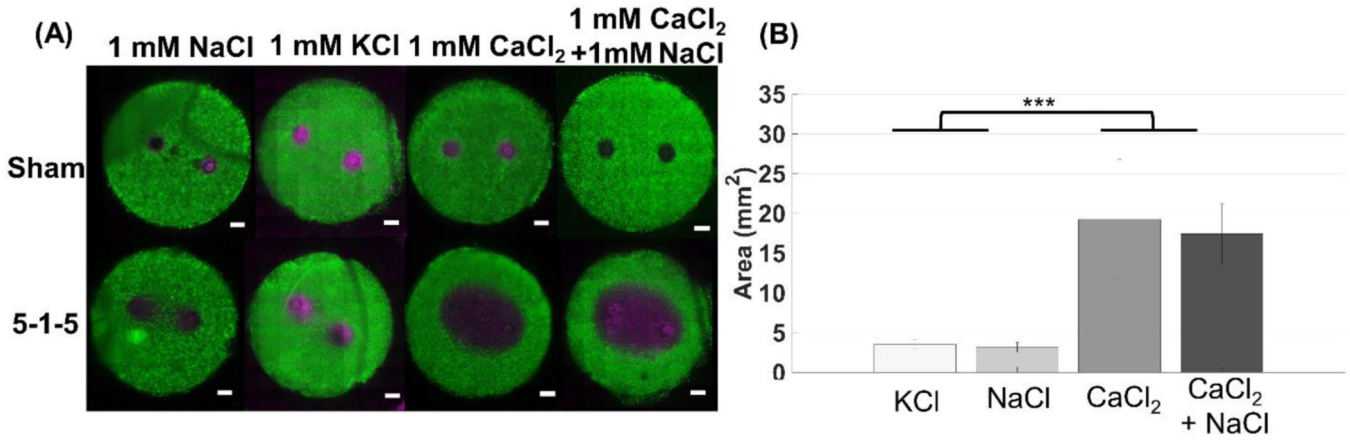

Figure 5: Enhanced cell death using H-FIRE treatment with pulse durations below 10 μs is unique to $CaCl_2$. Experiments were completed using a 5–1-5 waveform (*p < 0.001).**

(A) In vitro collagen scaffolds consisted of 5 mg/mL rat tail collagen type I and U251 malignant glioma cells (1×10^6 cells/mL). Electrodes were spaced 4 mm apart (center-to-center). 80 bursts consisting of 5 μs pulses were delivered at 800 V, frequency of 1 burst/second for a total on time of 100 μs. Live cells are stained with calcein AM (green) while dead and/or membrane compromised cells are stained with propidium iodide (magenta). Propidium iodide stains cells red, but the images are shown in magenta for visualization purposes. **(B)** Using a combined solution of 1mM $CaCl_2$ and 1 mM NaCl (n = 5) results in ablations similar in size to $CaCl_2$ alone (n = 9), therefore NaCl is unable to rescue the cells from the effect of $CaCl_2$. Replacing $CaCl_2$ with KCl (n = 8), results in an ablation that is similar to NaCl alone.

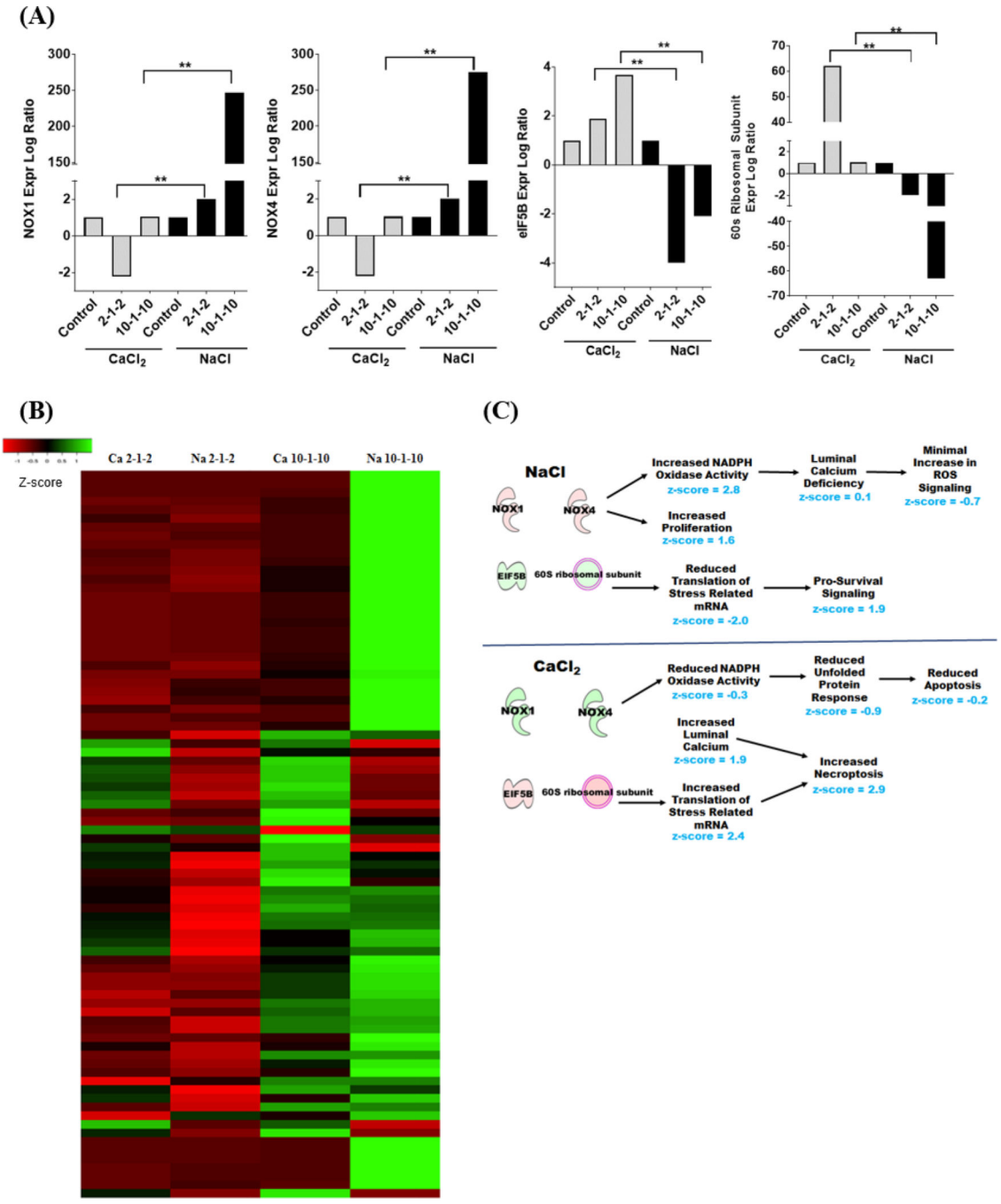

Figure 6: Signaling pathways associated with NOX1/4 and EIF5B are differentially regulated following H-FIRE depending on $CaCl_2$ or NaCl environment.

Gene expression profiling analysis identified biological functions specifically associated with NOX1, NOX4, EIF5B and the 60S ribosomal subunit that were significantly dysregulated following H-FIRE treatment and correlated with $CaCl_2$ or NaCl containing buffer. **(A)** Individual expression of each of these genes was significantly and differentially regulated based on $CaCl_2$ or NaCl. **(B)** Heatmap analysis reflects global changes in gene expression and revealed significant dysregulation among genes associated with NADPH

oxidase activity, proliferation, cell death, calcium signaling, and cellular stress. Red is downregulated genes and green signifies upregulated genes. **(C)** Ingenuity pathway analysis of gene expression profiling data revealed differentially activated pathways, quantified by associated z-score, associated with increased proliferation and survival under NaCl conditions and increased necroptosis under $CaCl_2$ conditions following H-FIRE. Here, red represents upregulated genes and green signifies downregulated genes. **$p < 0.01$.

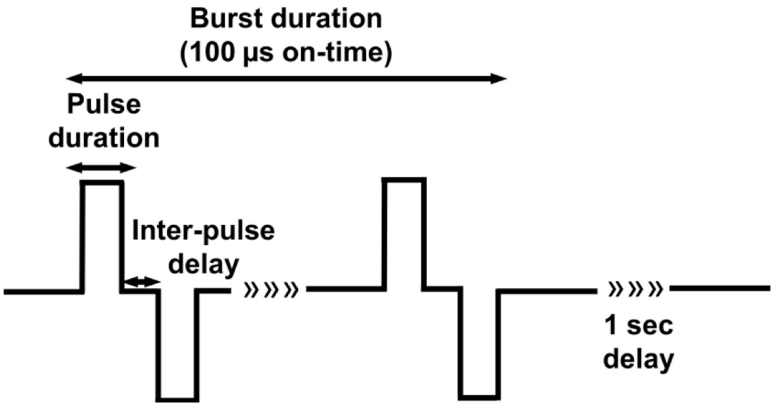

Schematic 1: Schematic of bipolar H-FIRE waveforms.

The same inter-pulse delay (1 µs) and varying pulse durations (1, 2, 5, 10 µs) were investigated in this study. A series of 80 bursts were delivered at the frequency of one burst/second and amplitude of 800 V for a total on time of 100 µs. H-FIRE waveforms are described in this study by the following name scheme (positive pulse duration – inter-pulse delay - negative pulse duration).

Table I:
Electric field threshold for both H-FIRE and IRE treatments.

Results are presented in V/cm as mean ± std (n ≥ 6 for all conditions). Boxes highlight that 10–1-10 H-FIRE treatment with calcium results in comparable electric field thresholds to standard IRE treatment.

		1-1-1	2-1-2	5-1-5	10-1-10	IRE
1mM NaCl	Irreversible	2481 ± 87	2382 ± 275	2282 ± 134	1641 ± 159	698 ± 103
	Reversible		1299 ± 119	1124 ± 175	839 ± 217	524 ± 85
1mM $CaCl_2$	Irreversible	2003 ± 270	1607 ± 112	1111 ± 208	771 ± 129	467 ± 67
	Reversible		954 ± 159	657 ± 67	577 ± 4	409 ± 57
5 mM NaCl	Irreversible	2494 ± 111	2331 ± 389	2197 ± 377	1597 ± 229	745 ± 139
	Reversible		1298 ± 206	1149 ± 148	804 ± 165	437 ± 88
5 mM $CaCl_2$	Irreversible	1702 ± 315	1222 ± 157	903 ± 145	871 ± 265	377 ± 19
	Reversible		900 ± 143	658 ± 36	578 ± 7	351 ± 53